

Article

# Microstructures and Properties Evolution of Al-Cu-Mn Alloy with Addition of Vanadium

Fansheng Meng, Zhi Wang, Yuliang Zhao, Datong Zhang and Weiwen Zhang \*

National Engineering Research Center of Near-net-shape Forming for Metallic Materials, South China University of Technology, Guangzhou 510640, China; mengfansheng@szpt.edu.cn (F.M.); wangzhi@scut.edu.cn (Z.W.); mezhaoYuliang@mail.scut.edu.cn (Y.Z.); dtzhang@scut.edu.cn (D.Z.)

\* Correspondence: mewzhang@scut.edu.cn; Tel.: +86-20-8711-2272

Academic Editor: Chun-Liang Chen

Received: 15 October 2016; Accepted: 23 December 2016; Published: 30 December 2016

**Abstract:** The effect of the vanadium addition on the microstructure, the precipitation behavior, and the mechanical properties of the Al-5.0Cu-0.4Mn alloy has been studied. The as-cast Al-5.0Cu-0.4Mn alloy was produced by squeeze casting and the heat treatment was carried out following the standard T6 treatment. It is shown that, with the addition of V, grain refinement of aluminum occurred. During heat treatment, the addition of V accelerates the precipitation kinetics of  $\theta'$  ( $\text{Al}_2\text{Cu}$ ) phase along the grain boundaries, and promotes the growth rate of the  $\theta'$  in the  $\alpha(\text{Al})$  matrix. Meanwhile, the addition of V retards the precipitation of T ( $\text{Al}_{20}\text{Cu}_2\text{Mn}_3$ ) phase. The tensile strength of the Al-5.0Cu-0.4Mn alloy increases with the increase of V content, which can be explained by combined effects of the solid solution strengthening and precipitate strengthening. However, excessively high V addition deteriorates the mechanical properties by forming brittle coarse intermetallic phases.

**Keywords:** Al alloys; mechanical properties; vanadium; squeeze casting; heat treatment

## 1. Introduction

Al-Cu-based alloys are one kind of important casting aluminum alloy, which have been widely used in aerospace, transportation, and other industries owing to their high strength, good heat resistance, and excellent machining performance [1–4]. The main strengthening effect in Al-Cu-based alloys results from the aging treatment, which gives rise to precipitate strengthening. The precipitation follows the sequence: GP zone  $\rightarrow \theta'' \rightarrow \theta' \rightarrow \theta$  ( $\text{Al}_2\text{Cu}$ ) [5]. It has been found that several precipitate characteristics—such as shape, size, density, and the degree of the coherency with the matrix—strongly influence the strength and ductility of the Al-Cu-based alloy. For example, the  $\theta'$  precipitate, which is only partially coherent with the matrix, shows the highest strengthening effect in Al-Cu-based alloys [5]. Nowadays, simple Al-Cu alloys are not widely used and are more and more being replaced by the wrought alloys and casting alloys through micro-alloying with other elements. The common added alloying elements in Al-Cu alloys are Mg, Si, and Zn, which are effective to change the precipitation behavior and thereby improve the mechanical properties [6–10]. In general, the effects of the micro-alloying elements on the precipitation behavior—such as rare earth metals, Zr, V, Sc, Ti, Mn—can be classified into two types: one promotes the precipitation of the hardening particles and the other one forms new precipitates with the matrix and/or other elements [11–16].

Recently, V was found to be a promising additive in Al alloys. It has been proven that an appreciate addition of V in Al-based alloys can significantly increase the strength without losing much ductility [17]. For example, Elhadari et al. [18] reported that the ultimate tensile strength and yield strength of the T6 condition (T6 peak-aged condition is one of the major factors to enhance mechanical properties of the alloy through an optimization of both the solution heat treatment and the artificial

aging conditions applied to the alloy [19]) were significantly improved by adding 0.25 wt. % V into the Al-7.0Si-1.0Cu-0.5Mg-0.1Ti-0.2Zr alloy, while the elongation of the alloy decreased slightly. The main strengthening mechanism is attributed to grain refinement according to the Hall-Petch relationship, where the addition of V in Al alloys can refine the grain size [20,21]. The possible reason for the grain refinement is that V can promote the heterogeneous nucleation during solidification. In addition, constituent intermetallics such as Al<sub>10</sub>V and Al<sub>3</sub>V may form during the aging heat treatment [22]. However, most of these studies focused on Al-Si and Al-Mg based alloys, and the effect of the addition of V on the precipitation behavior and mechanical properties of Al-Cu based alloys is still not clear.

In this work, a systematic work was performed to investigate the effect of V addition on microstructural evolution and tensile properties of the squeeze casted Al-5.0Cu-0.4Mn alloys in as-cast and heat-treated conditions. The addition of 0.4 wt. % Mn can form strengthening phases, and play adispersion strengthening effect, which can improve the mechanical properties of Al-5.0Cu-based alloys [23–26]. Squeeze casting is a common method for preparing high performance materials and components because of the reduction of the shrinkage and thermal crack defects in the alloy [27–29], where high densification samples can be obtained.

## 2. Materials and Methods

A series of high purity-based Al-5.0 wt. % Cu-0.4 wt. % Mn alloys with various additions of V, as listed in Table 1, were prepared by melting the raw materials in a resistance furnace then casting into steel molds in air. The raw materials were 99.95 wt. % purity aluminum, Al-50 wt. % Cu, Al-10 wt. % Mn, and Al-5 wt. % V master alloys. The alloys were melted in a resistance furnace and kept at 903 K for about 5 min, and then the melt was poured manually into a steel mold preheated to 473 K and a pressure of 100 MPa was applied for 30 s. The cast billets have a weight of about 1 kg and a size of about  $\Phi 80$  mm  $\times$  100 mm. Solid solution heat treatment was performed at 540 °C for 12h, and the artificial aging treatment was performed at 175 °C for 8 h.

**Table 1.** Chemical composition (wt. %) and grain size of the alloys.

Designation Alloys	Element (wt. %) Cu Mn V Al				Grain Size( $\mu$ m)
Al-5.0Cu-0.4Mn	4.58	0.43	0	Balance	800
Al-5.0Cu-0.4Mn-0.05V	4.57	0.40	0.04	Balance	720
Al-5.0Cu-0.4Mn-0.15V	4.52	0.39	0.15	Balance	665
Al-5.0Cu-0.4Mn-0.25V	4.56	0.40	0.27	Balance	610
Al-5.0Cu-0.4Mn-0.40V	4.47	0.40	0.40	Balance	535
Al-5.0Cu-0.4Mn-0.55V	4.71	0.42	0.56	Balance	450

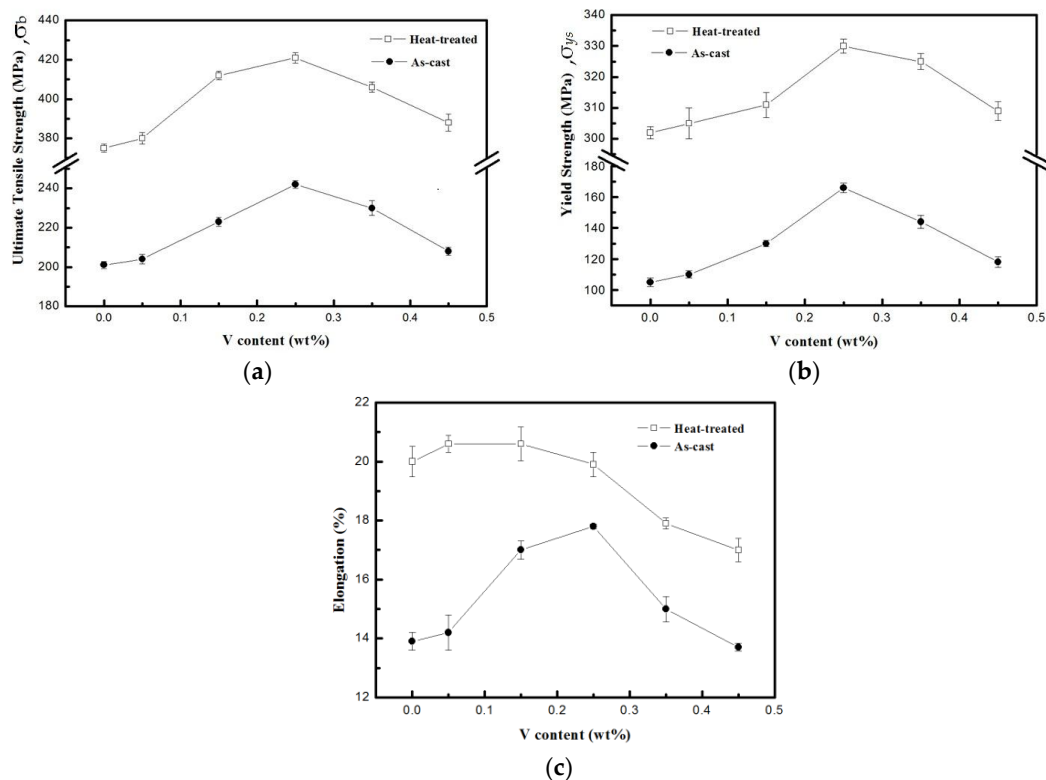
For comparison, all the samples were chosen from the same position (center) of the cast billets. Cylindrical tensile specimens were machined with a gauge length of 25 and a diameter of 5 mm. The tensile tests were performed at room temperature using a universal testing machine (SANS CMT5105, MTS, Eden Prairie, MN, USA) with a strain rate of 1mm/min. Three samples were tested for each condition to confirm reproducibility. The sample for the scanning electron microscopy (SEM) was etched with Keller reagent (Nanhai Zhili Chemical, Foshan, China), and observed using a Quanta 2000 SEM (FEI, Hillsboro, OR, USA) equipped with an energy-dispersive X-ray spectroscopy (EDX, FEI, Hillsboro, OR, USA) setup. The spectral analysis was carried on a microprobe analyzer EPMA-1600 (SHIMADZU, Kyoto, Japan). Transmission electron microscope (TEM) samples were prepared by twin-jet electropolishing with a solution for 3:7 volume ratio of HNO<sub>3</sub> in methanol solution at temperature of  $-25^{\circ}$ C and examined in a JEM-2200FS TEM (JEOL, Tokyo, Japan) operating at voltage of 200 kV. Optical images were obtained using a LEICA/DMI 5000M optical microscopy (OM, Leica, Solms, Germany). The diameter of the grains of the alloys was measured using OM images. The width of the grain boundaries and the length of  $\theta'$  phase was measured manually using at least

five TEM images. At least 20 counts for the grain boundary and 100 counts for the length of  $\theta'$  phase were done for each alloy.

### 3. Results

#### 3.1. Mechanical Properties

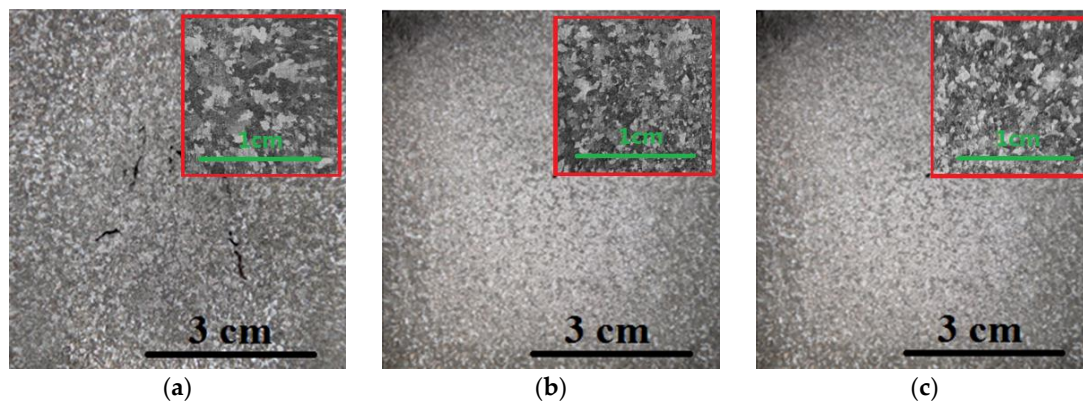
The average values of the tensile properties of as-cast and heat-treated alloys are summarized in Figure 1. It is clear that the addition of V strongly influences the tensile properties of the Al-5.0Cu-0.4Mn alloys in both as-cast and heat-treated conditions. With increasing V content, both ultimate tensile strength ( $\sigma_b$ ) and yield strength ( $\sigma_{ys}$ ) increase at first and then decrease at higher V content. The alloy with addition of 0.25 wt. % V exhibits the best mechanical properties under both conditions. For the as-cast alloy the  $\sigma_b$  and  $\sigma_{ys}$  is 242 MPa and 166 MPa, respectively, while for the heat-treated alloy, the  $\sigma_b$  and  $\sigma_{ys}$  is 421 MPa and 330 MPa, respectively. The elongation of the heat-treated alloys decreases from 20% for the alloy without V addition to 17% for the alloy with addition of 0.55 wt. % V. For the as-cast alloys, the elongation increases from 14% for the alloy without V addition to 18% for the alloy with addition of 0.25 wt. % V, and then decreases to 14% for the alloy with addition of 0.55 wt. % V.



**Figure 1.** Tensile properties of the alloys in as-cast and heat-treated conditions: (a) ultimate tensile strength; (b) yield strength; (c) elongation.

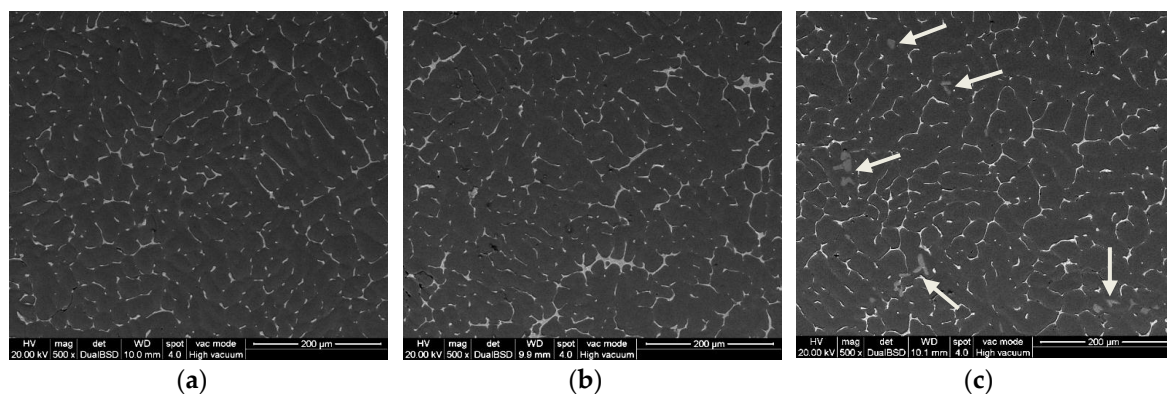
#### 3.2. Microstructure

Figure 2 shows the central part of the as-cast Al-5.0Cu-0.4Mn alloys with different contents of V. Figure 2a–c is obtained by SLR camera, and Figure 2d–f is obtained by optical micrography. It can be seen that the grain size of the Al-5.0Cu-0.4Mn alloys decreases with increasing content of V. For example, the average grain size of the alloy with the addition of 0.55 wt. % V is 450  $\mu\text{m}$ , which is nearly two times smaller than the alloy without the addition of V, as shown in Table 1. However, shrinkage voids were observed in the center due to the relatively large-size ingots. To avoid these defects of shrinkage voids, higher pressure or smaller samples are required during squeeze casting.



**Figure 2.** Optical images of the as-cast alloys with: (a) 0 wt. % V; (b) 0.25 wt. % V; (c) 0.55 wt. % V. The insets correspond to the higher magnification images taken from the position close to the surface of the ingots.

Figure 3 shows SEM micrographs of the alloys. Typical as-cast  $\alpha(\text{Al})$  dendrites (dark areas in Figure 3a–c) were observed, where the bright phases distribute along the boundaries. Most of these bright phases were likely  $\theta$  ( $\text{Al}_2\text{Cu}$ ) phase according to the EDX result, in which the atomic ratio of Al:Cu was 71:29. For the as-cast alloy with the addition of 0.25 wt. % V, no V-rich coarse phase is found (Figure 3b). With the V content increasing to 0.55 wt. %, the primary  $\text{Al}_{10}\text{V}$  phase, is found in the as-cast  $\alpha(\text{Al})$  dendrites with a size of tens of micrometers (Figures 3c and 4a). The diameter of the equivalent circle of  $\text{Al}_{10}\text{V}$  is  $\sim 21 \mu\text{m}$ , where the size distribution is shown in Table 2. The primary  $\text{Al}_{10}\text{V}$  phase can act as heterogeneous particles for the formation of  $\alpha$ -Al grains, which plays a role in the grain refinement. Figure 3d,e shows SEM images of the heat-treated samples with 0 and 0.25 wt. % V, respectively, indicating that the second  $\theta$  phase dissolve during solid solution heat treatment. After artificial aging, the solute elements might be dissolved into the  $\alpha(\text{Al})$  matrix and other phases. Another possibility for the solute elements is that they form GP zones, dispersion, or precipitates in the  $\alpha(\text{Al})$  matrix. To address this issue, TEM observations were performed and the results are shown below. When the V content is increased to 0.55 wt. %, the coarse  $\text{Al}_{10}\text{V}$  phase which were formed during casting still remain in the  $\alpha(\text{Al})$  matrix after the T6 heat treatment (Figure 3f). Figure 4 shows EDX of the  $\text{Al}_{10}\text{V}$  phase, revealing the presence of a relatively high content of Mn ( $3.0 \pm 0.5 \text{ at. } \%$ ) in the  $\text{Al}_{10}\text{V}$  phase, which is much higher than that in the  $\alpha(\text{Al})$  matrix which is  $0.19 \pm 0.05 \text{ at. } \%$ . The content of Cu in the  $\text{Al}_{10}\text{V}$  phase is  $2.0 \pm 0.8 \text{ at. } \%$ , which may partially originate from the high concentration of Cu in the matrix.



**Figure 3.** Cont.

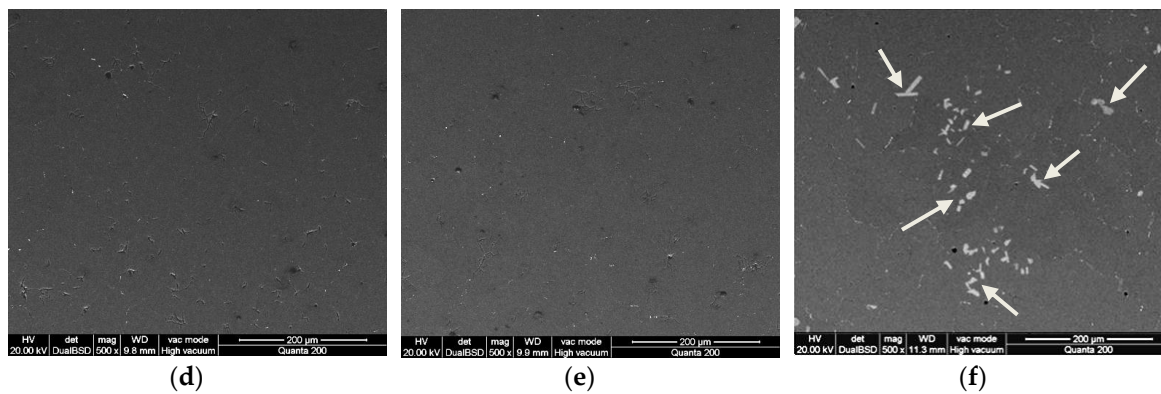


**Figure 3.** SEM micrographs in backscattered electron (BSE) mode showing the as-cast alloys with: (a) 0 wt. % V; (b) 0.25 wt. % V; (c) 0.55 wt. % V and heat-treated alloys with: (d) 0 wt. % V; (e) 0.25 wt. % V; (f) 0.55 wt. % V. The white arrows show the  $Al_{10}V$  phase.

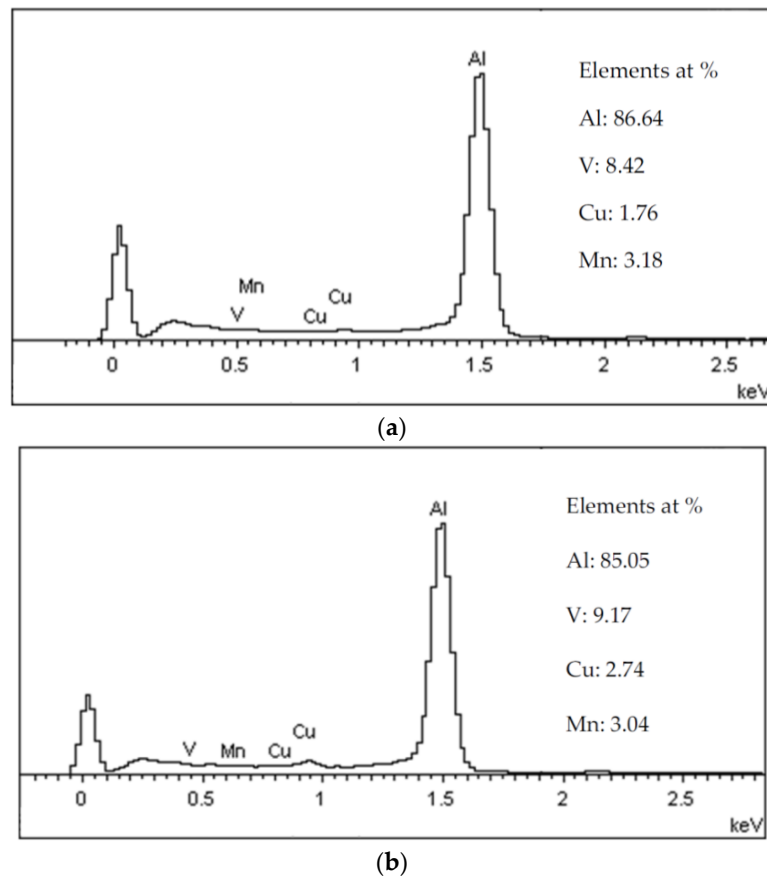


**Figure 4.** EDX of coarse  $Al_{10}V$  phase in the alloys with addition of 0.55 wt. % V: (a) as-cast; (b) heat-treated.

**Table 2.** Size distribution of the  $Al_{10}V$  phase in the as-cast alloy with addition of 0.55 wt. % V.

Size Distribution	<20 $\mu m$	20 $\mu m$ –30 $\mu m$	30 $\mu m$ –40 $\mu m$	>40 $\mu m$
Quantity Proportion	62%	24%	11%	3%

Figures 5 and 6 show representative bright-field TEM images of the heat-treated alloys with and without the addition of V, showing different features due to different incident beam directions.

The formation of  $\theta'$  precipitates with long shape after T6 heat treatment was observed, where the EDX analysis shows that the Al/Cu atomic ratio is close to 2 (Figure 7a). This is in agreement with the characteristic shape of the  $\theta'$  which was reported in Al-Cu based alloys. With increasing V content, an increased number of  $\theta'$  precipitates can clearly be seen in the grain boundaries (shown by the arrows in Figure 5a–c), where the width of the grain boundary increases from  $\sim 0.01$  at 0 wt. % V to  $0.06 \pm 0.01$  and  $0.13 \pm 0.04$   $\mu\text{m}$  at 0.25 wt. % V and 0.55 wt. % V, respectively. Furthermore, the size of the  $\theta'$  precipitates in the  $\alpha(\text{Al})$  matrix increased with increasing V content (Figure 5d–f). For example, the length of the  $\theta'$  precipitates increases from  $30 \pm 10$  at 0 wt. % V to  $60 \pm 15$  and  $100 \pm 20$  nm at 0.25 wt. % V and 0.55 wt. % V, respectively. This can be explained by the acceleration effect of V on the precipitation kinetics [30]. The solid solution of V in the different alloys increases with increasing V content in both as-cast and heat-treated conditions, as shown in Table 3.

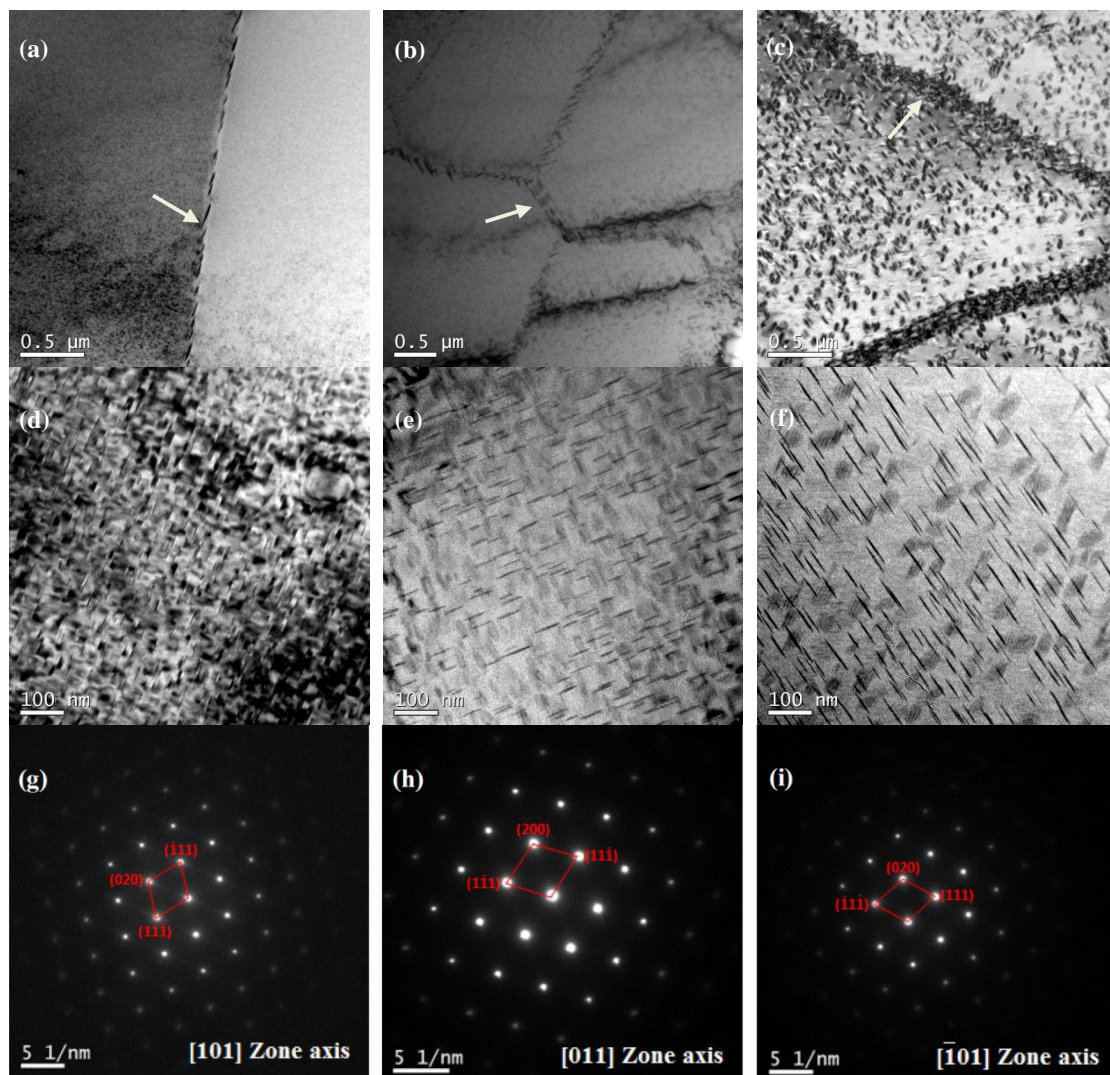


**Figure 5.** TEM micrographs of the  $\theta'$  ( $\text{Al}_2\text{Cu}$ ) phase in the heat-treated alloys with different additions of V: (a), (d) 0 wt. % V and (g) selected-area electron diffraction (SAED) pattern of  $\alpha(\text{Al})$  matrix in (d); (b), (e) 0.25 wt. % V and (h) SAED pattern of  $\alpha(\text{Al})$  matrix in (e); (c), (f) 0.55 wt. % V and (i) SAED pattern of  $\alpha(\text{Al})$  matrix in (f). The white arrows show the grain boundaries.

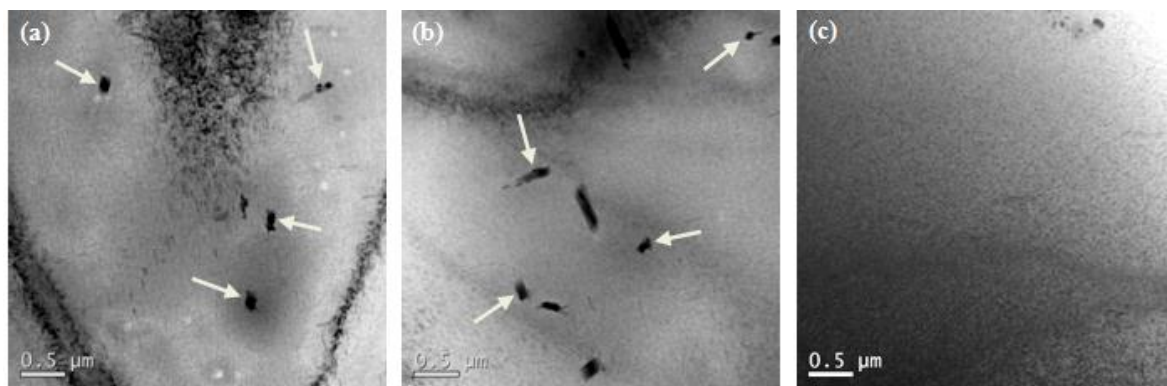


**Figure 6.** TEM micrographs of the T ( $\text{Al}_{20}\text{Cu}_2\text{Mn}_3$ ) phase in the heat-treated alloys with different additions of V: (a) 0 wt. % V; (b) 0.25 wt. % V; (c) 0.55 wt. % V. The white arrows show the T phase.

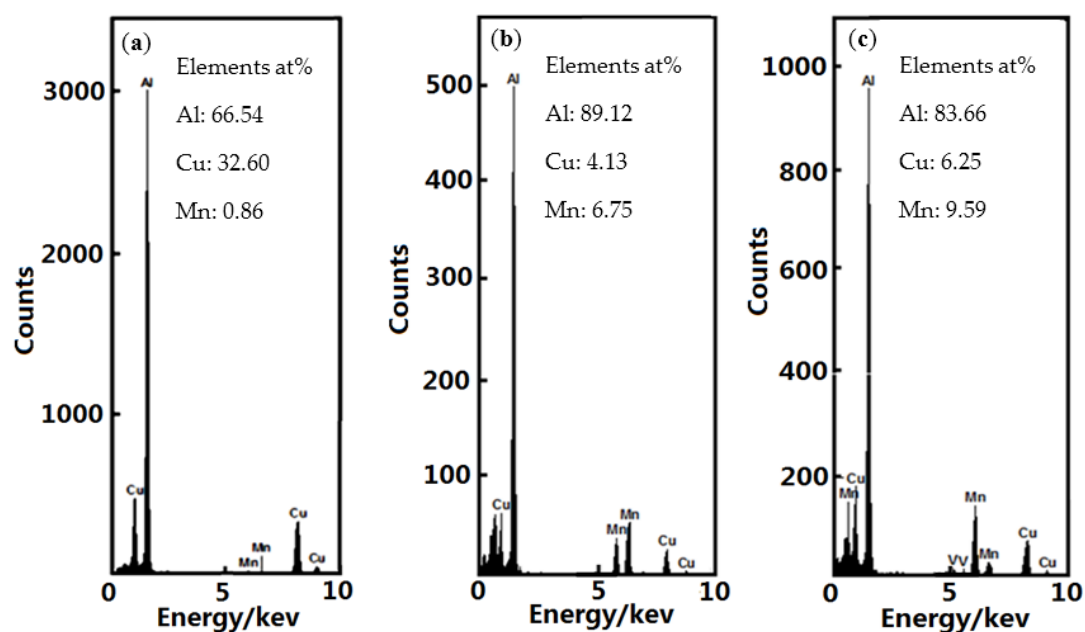


**Figure 7.** EDX analysis of the precipitated phase in TEM micrographs: (a)  $\theta'$  phase shown in Figure 5f; (b) T phase shown in Figure 6a; (c) T phase shown in Figure 6b.

**Table 3.** The V content (wt. %) in the  $\alpha(\text{Al})$  matrix of the alloys.

Designation Alloys	As-Cast Alloys	Heat-Treated Alloys
Al-5.0Cu-0.4Mn	0	0
Al-5.0Cu-0.4Mn-0.05V	$0.07 \pm 0.03$	$0.06 \pm 0.04$
Al-5.0Cu-0.4Mn-0.15V	$0.19 \pm 0.05$	$0.16 \pm 0.04$
Al-5.0Cu-0.4Mn-0.25V	$0.32 \pm 0.06$	$0.28 \pm 0.07$
Al-5.0Cu-0.4Mn-0.55V	$0.38 \pm 0.07$	$0.32 \pm 0.06$

Another precipitate phase shown, in the alloys without V and with 0.25 wt. % V (Figure 6a,b), is identified as the T ( $\text{Al}_{20}\text{Cu}_2\text{Mn}_3$ ) phase according to the EDX results and related references (Figure 7b,c) [31,32]. However, T phase is not seen in the  $\alpha(\text{Al})$  matrix of the alloy with the addition of 0.55 wt. % V (Figure 6c), indicating that its formation is thermodynamically limited when V is added. This is likely due to the relatively high solid solubility of Mn,  $\sim 5$  wt. %, in the coarse  $\text{Al}_{10}\text{V}$  phase in the alloy with the addition of 0.55 wt. % V (Figure 3), which will lead to dissolution of the Mn concentration in the  $\alpha(\text{Al})$  matrix and this limit of the formation of Mn-enriched phase.

### 3.3. Fractographic Observations

Figure 8 shows details of the fracture profiles of the alloys with different V contents. For the as-cast alloys, fracture initiates at the grain boundaries due to both debonding and cracking of the brittle intermetallics. Once the tensile load reaches the critical value where some microcracks link with each other, the principal crack is formed along the grain boundaries, leading to intergranular fracture. On the other hand, transgranular fracture is observed in the heat-treated alloys. Crack initiation at the coarse  $Al_{10}V$  phase is observed in the heat-treated alloy with addition of 0.55 wt. % V, which significantly decreases the strength and ductility. Figure 9 shows the fracture surface of the heat-treated alloys after tensile deformation. Ductile fracture with many dimples is observed in the fracture surface. Additionally, the failure of the coarse  $Al_{10}V$  phase was also found at the fracture surface (marked as arrows in Figure 9c), which is in accordance with the SEM observation in Figure 8f.

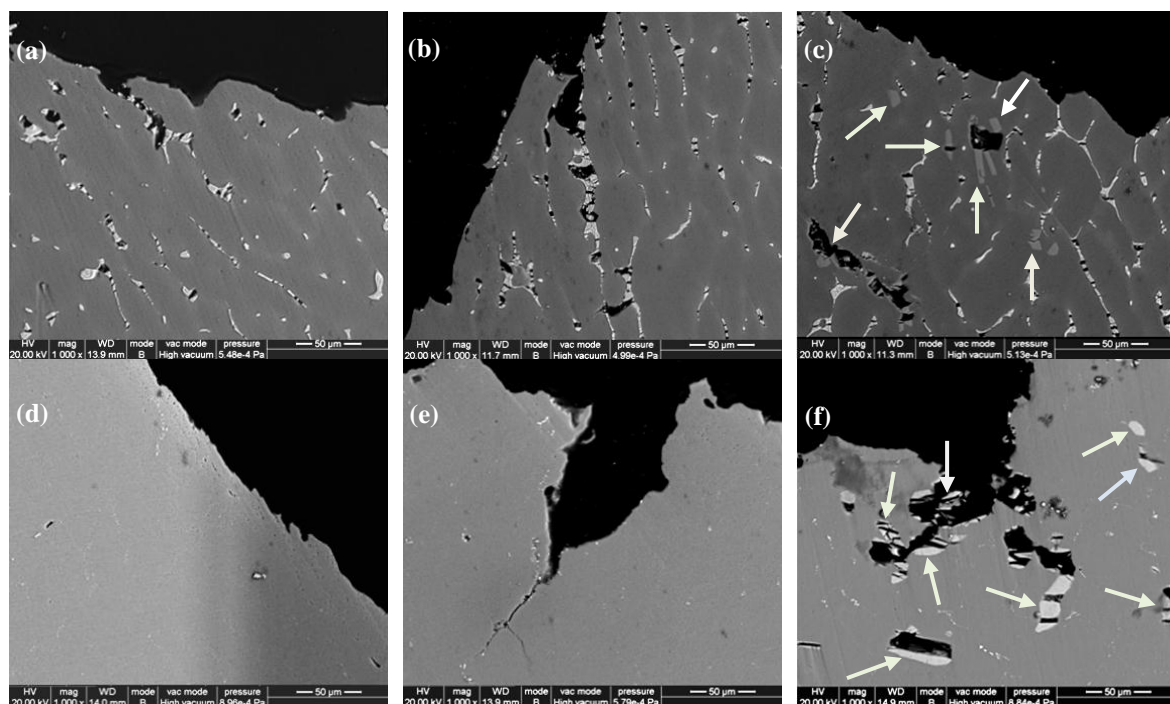


**Figure 8.** SEM micrographs in BSE mode showing the fracture profiles of as-cast alloys with: (a) 0 wt. % V; (b) 0.25 wt. % V; (c) 0.55 wt. % V and heat-treated alloys with: (d) 0 wt. % V; (e) 0.25 wt. % V; (f) 0.55 wt. % V. The white arrows show the  $Al_{10}V$  phase.

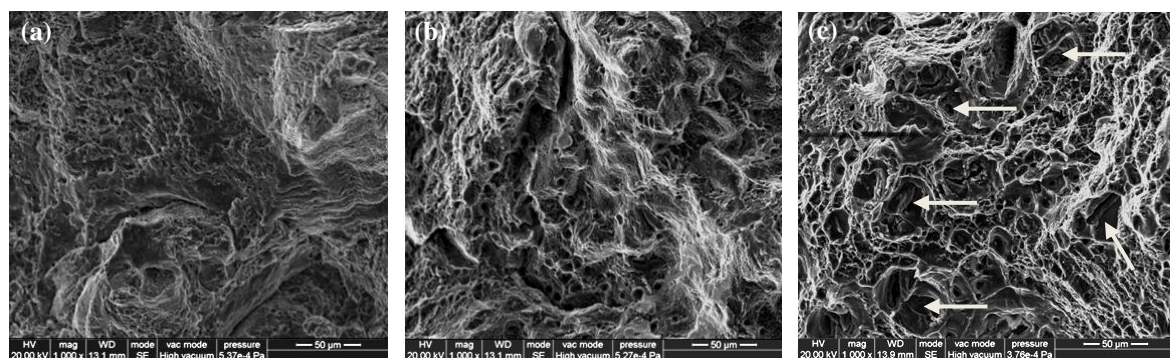


**Figure 9.** SEM micrographs in BSE mode showing the fracture surface of the heat-treated alloys with: (a) 0 wt. % V; (b) 0.25 wt. % V; (c) 0.55 wt. % V. The white arrows show the failure of the coarse  $Al_{10}V$  phase.

#### 4. Discussion

This work has shown that an appropriate V addition increases the strength of the Al-5.0Cu-0.4Mn alloys in both as-cast and heat-treated conditions. On a weight basis, the optimum V content is ~0.25 wt. % for the Al-5.0Cu-0.4Mn alloy, which shows the highest strength and good ductility. For the as-cast alloys, the strength increment is most likely attributed to the solid solution strengthening (Table 3), while the precipitate strengthening may also play a role on the strength. However, excessive addition of V decreases the strength of the as-cast alloys due to the formation of a coarse brittle Al<sub>10</sub>V phase, resulting in crack initiation and crack propagation. The elongation of the as-cast alloy changes little when the V content increases to 0.25 wt. %, whereas it decreases quickly at V content of 0.55 wt. % due to the fracture of the coarse Al<sub>10</sub>V phase.

After heat treatment, the precipitation of fine semi-coherent  $\theta'$  precipitates in the  $\alpha$ (Al) matrix exerts a strong strengthening effect on the Al-5.0Cu-0.4Mn alloys with and without V addition, resulting in significant strength improvement compared to the as-cast alloys (Figure 1). The explanation for the increased strength in the heat-treated alloys with increasing V content lies largely in the strengthening effects caused by solid solution strengthening and precipitate strengthening. Although, with increasing V content, increased precipitate  $\theta'$  density along the grain boundaries (Figure 5a–c) may lead to some strengthening effect by retarding the dislocation movement, the grain boundary strengthening due to the grain refinement might be weak when the grains are as big as hundreds of micrometers. It is found that the solid solution level of V increases in the alloys with higher V content, indicating that solid solution strengthening occurs. In addition, it is evident that precipitate strengthening plays an important role in the strengthening effect in the heat-treated alloys. However, the effect of V addition on precipitate strengthening is still not clarified by this work alone and it will be further investigated in future work.

As shown above, a coarse Al<sub>10</sub>V phase form during solidification and remain in the heat-treated alloys when a high V content was added. Therefore, the strength of the high V-containing alloy decreases owing to the early failure of the coarse Al<sub>10</sub>V phase. In addition, the coarse Al<sub>10</sub>V phase significantly deteriorates the ductility of the alloys. For the alloys with addition of 0.25 wt. % V or less, they exhibit necking due to the localized plastic deformation and then break at the plane having ~45° with respect to the tensile axis, which is along the plane of maximum shear stress (Figure 10a,b,d,e). This is a typical fracture of ductile or semi-ductile materials. Whereas the alloy with addition of 0.55 wt. % V exhibits a small necking and rough fracture surface which is closely perpendicular to the tensile axis (Figure 10c,f), indicating that it fails in a brittle way. The main reason is that the coarse Al<sub>10</sub>V intermetallic phase cracks at a low plastic strain and provides low energy sites for the initiation and growth of cracks under uniaxial tension. With further deformation, these cracks propagate and interconnect each other which finally results in failure of the alloy at the cross-section which has the shortest distance within the tensile sample.

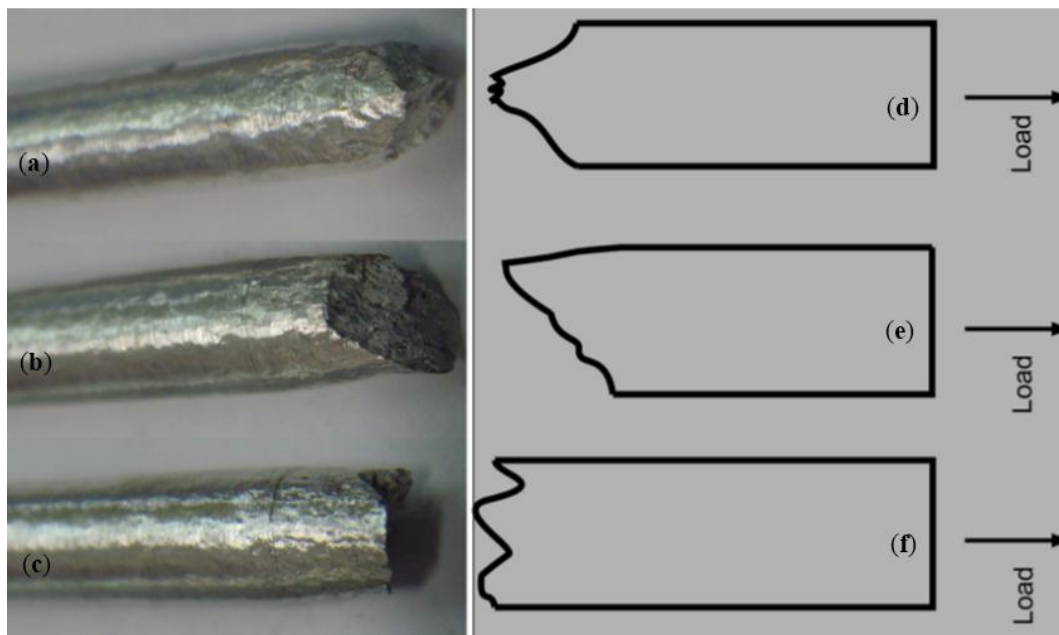


**Figure 10.** Tensile tested samples after fracture: (a) 0 V; (b) 0.25 wt. %; (c) 0.55 wt. %; (d–f) are the schematic diagrams of the fracture mode corresponding to (a–c) respectively.

## 5. Conclusions

The effect of V on the microstructure and tensile properties of Al-5.0Cu-0.4Mn alloy in as-cast and heat-treated conditions was investigated. The following conclusions can be drawn from this work:

The addition of V changes the precipitation behavior of the Al-5.0Cu-0.4Mn alloy, accelerating the precipitation kinetics of  $\theta'$  phase along the grain boundaries, and promoting the growth rate of the  $\theta'$  in the  $\alpha$ (Al) matrix. Meanwhile, the addition of V retards the precipitation of T phase.

V significantly influences the tensile properties of the alloys in both as-cast and heat-treated conditions. The addition of V initially leads to a strength increment and then a decrease in strength. The strength of the alloy reaches a peak level in both as-cast and heat-treated conditions when 0.25 wt. % V is added. The heat-treated alloy, with the addition of 0.25 wt. % V, exhibits the best mechanical properties with  $\sigma_b$ ,  $\sigma_{ys}$  and elongation of 421 MPa, 330 MPa and 18%, respectively, which is 12.3%, 9.3%, and 28.1% higher than the heat-treated alloy without V addition.

The strengthening mechanisms for the as-cast alloy containing V can mostly be explained by the solid solution strengthening. The strengthening mechanisms for the heat-treated alloy containing V can be explained as solid solution strengthening and precipitate strengthening.

**Acknowledgments:** This work was sponsored by National Natural Science Foundation of China (No. 51374110); Major Special Project for Science and Technology of Guangdong Province (No. 2015B090926004); and Guangdong Natural Science Foundation for Research Team (No. 2015A030312003).

**Author Contributions:** Fansheng Meng performed the experiments; Zhi Wang and Datong Zhang wrote and edited the manuscript; Yuliang Zhao analyzed the data; Weiwen Zhang conceived and designed the experiments, and contributed to all activities.

**Conflicts of Interest:** The authors declare no conflict of interest.

## References

1. Sistaninia, M.; Terzi, S.; Phillion, A.B.; Drezet, J.-M.; Rappaz, M. 3-D granular modeling and in situ X-ray tomographic imaging: A comparative study of hot tearing formation and semi-solid deformation in Al-Cu alloys. *Acta Mater.* **2013**, *61*, 3831–3841. [[CrossRef](#)]

2. Jang, J.H.; Nam, D.G.; Park, Y.H.; Park, I.M. Effect of solution treatment and artificial aging on microstructure and mechanical properties of Al-Cu alloy. *Trans. Nonferr. Met. Soc. China* **2013**, *23*, 631–635. [[CrossRef](#)]
3. McKeown, J.T.; Kulovits, A.K.; Liu, C.; Zwiack, K.; Reed, B.W.; LaGrange, T.; Wieszorek, J.M.K.; Campbell, G.H. In situ transmission electron microscopy of crystal growth-mode transitions during rapid solidification of a hypoeutectic Al-Cu alloy. *Acta Mater.* **2014**, *65*, 56–58. [[CrossRef](#)]
4. Zhang, W.; Lin, B.; Zhang, D.; Li, Y. Microstructures and mechanical properties of squeeze cast Al-5.0Cu-0.6Mn alloys with different Fe content. *Mater. Des.* **2013**, *52*, 225–233. [[CrossRef](#)]
5. Totten, G.E.; MacKenzie, D.S. *Handbook of Aluminum: Vol. 1: Physical Metallurgy and Processes*; CRC Press: Boca Raton, FL, USA, 2003.
6. Wang, S.C.; Starink, M.J. Two types of S phase precipitates in Al-Cu-Mg alloys. *Acta Mater.* **2007**, *55*, 933–941. [[CrossRef](#)]
7. Ferreira, I.L.; Garcia, A.; Nestler, B. On macrosegregation in ternary Al-Cu-Si alloys: Numerical and experimental analysis. *Scr. Mater.* **2004**, *50*, 407–411. [[CrossRef](#)]
8. Fan, X.; Jiang, D.; Meng, Q.; Zhong, L. The microstructural evolution of an Al-Zn-Mg-Cu alloy during homogenization. *Mater. Lett.* **2006**, *60*, 1475–1479. [[CrossRef](#)]
9. Kamga, H.K.; Larouche, D.; Bournane, M.; Rahem, A. Mechanical properties of aluminium-copper B206 alloys with iron and silicon additions. *Int. J. Cast Met. Res.* **2012**, *25*, 17–25. [[CrossRef](#)]
10. Wang, S.C.; Starink, M.J.; Gao, N. Precipitation hardening in Al-Cu-Mg alloys revisited. *Scr. Mater.* **2006**, *54*, 287–291. [[CrossRef](#)]
11. Yang, C.; Zhang, P.; Shao, D.; Wang, R.; Cao, L.; Zhang, J.; Liu, G.; Chen, B.; Sun, J. The influence of Sc solute partitioning on the microalloying effect and mechanical properties of Al-Cu alloys with minor Sc addition. *Acta Mater.* **2016**, *119*, 68–79. [[CrossRef](#)]
12. Zhang, W.; Lin, B.; Cheng, P.; Zhang, D.; Li, Y. Effects of Mn content on microstructures and mechanical properties of Al-5.0Cu-0.5Fe alloys prepared by squeeze casting. *Trans. Nonferrous Met. Soc. China* **2013**, *23*, 1525–1531. [[CrossRef](#)]
13. Mahmudi, R.; Sepehrband, P.; Ghasemi, H.M. Improved properties of A319 aluminum casting alloy modified with Zr. *Mater. Lett.* **2006**, *60*, 2606–2610. [[CrossRef](#)]
14. Wu, Y.; Liao, H.; Zhou, K. Effect of minor addition of vanadium on mechanical properties and microstructures of as-extruded near eutectic Al-Si-Mg alloy. *Mater. Sci. Eng. A* **2014**, *602*, 41–48. [[CrossRef](#)]
15. Shaha, S.K.; Czerwinski, F.; Kasprza, W.; Friedman, J.; Chen, D.L. Effect of Zr, V and Ti on hot compression behavior of the Al-Si cast alloy for powertrain applications. *J. Alloy. Compd.* **2014**, *615*, 1019–1031. [[CrossRef](#)]
16. Vončina, M.; Medved, J.; Bončina, T.; Zupanič, F. Effect of Ce on morphology of  $\alpha$ (Al)-Al<sub>2</sub>Cu eutectic in Al-Si-Cu alloy. *Trans. Nonferr. Met. Soc. China* **2014**, *24*, 36–41. [[CrossRef](#)]
17. Casari, D.; Ludwig, T.H.; Merlin, M.; Arnberg, L.; Garagnani, G.L. The effect of Ni and V trace elements on the mechanical properties of A356 aluminium foundry alloy in as-cast and T6 heat treated conditions. *Mater. Sci. Eng. A* **2014**, *610*, 414–426. [[CrossRef](#)]
18. Elhadari, H.A.; Patel, H.A.; Chen, D.L.; Kasprzak, W. Tensile and fatigue properties of a cast aluminum alloy with Ti, Zr and V additions. *Mater. Sci. Eng. A* **2011**, *528*, 8128–8138. [[CrossRef](#)]
19. Mahathaninwong, N.; Plookphola, T.; Wannasina, J.; Wisutmethangoon, S. T6 heat treatment of rheocasting 7075 Al alloy. *Mater. Sci. Eng. A* **2012**, *532*, 91–99. [[CrossRef](#)]
20. Haghayeghi, R.; Kapranos, P. Comparison on grain refinement efficiency of peritectic and eutectic alloying elements on pure Aluminium. *Met. Mater. Int.* **2014**, *20*, 713–717. [[CrossRef](#)]
21. Wang, F.; Liu, Z.; Qiu, D.; Taylor, J.A.; Easton, M.A.; Zhang, M. Revisiting the role of peritectics in grain refinement of Al alloys. *Acta Mater.* **2013**, *61*, 360–370. [[CrossRef](#)]
22. Meng, Y.; Cui, J.; Zhao, Z.; Zuo, Y. Effect of vanadium on the microstructures and mechanical properties of an Al-Mg-Si-Cu-Cr-Ti alloy of 6XXX series. *J. Alloy. Compd.* **2013**, *573*, 102–111. [[CrossRef](#)]
23. Hwanga, J.Y.; Doty, H.W.; Kaufman, M.J. The effects of Mn additions on the microstructure and mechanical properties of Al-Si-Cu casting alloys. *Mater. Sci. Eng. A* **2008**, *488*, 496–504. [[CrossRef](#)]
24. Huang, H.; Cai, Y.; Cui, H.; Huang, J.; He, J.; Zhang, J. Influence of Mn addition on microstructure and phase formation of spray-deposited Al-25Si-xFe-yMn alloy. *Mater. Sci. Eng. A* **2009**, *502*, 118–125. [[CrossRef](#)]
25. Tsivoulas, D.; Prangnell, P.B. The effect of Mn and Zr dispersoid-forming additions on recrystallization resistance in Al-Cu-Li AA2198 sheet. *Acta Mater.* **2014**, *77*, 1–16. [[CrossRef](#)]

26. Fan, L.; Hao, Q.; Han, W. Dual characteristic of trace rare earth elements in a commercial casting Al-Cu-X alloy. *Rare Met.* **2015**, *34*, 308–313. [[CrossRef](#)]
27. Ghomashchi, M.R.; Vikhrov, A. Squeeze casting: An overview. *J. Mater. Process. Technol.* **2000**, *101*, 1–9. [[CrossRef](#)]
28. Maleki, A.; Niroumand, B.; Shafyei, A. Effects of squeeze casting parameters on density, macrostructure and hardness of LM13 Alloy. *Mater. Sci. Eng. A* **2006**, *428*, 135–140. [[CrossRef](#)]
29. Zhang, W.; Lin, B.; Fan, J.; Zhang, D.; Li, Y. Microstructures and mechanical properties of heat-treated Al-5.0Cu-0.5Fe squeeze cast alloys with different Mn/Fe ratio. *Mater. Sci. Eng. A* **2013**, *588*, 366–375. [[CrossRef](#)]
30. Camero, S.; Puchi, E.S.; Conzalez, G. Effect of 0.1% vanadium addition on precipitation behavior and mechanical properties of Al-6063 commercial alloy. *J. Mater. Sci.* **2006**, *41*, 7361–7373. [[CrossRef](#)]
31. Chen, Y.; Yi, D.; Jiang, Y.; Wang, B.; Xu, D.; Li, S. Twinning and orientation relationships of T-phase precipitates in an Al matrix. *J. Mater. Sci.* **2013**, *48*, 3225–3231. [[CrossRef](#)]
32. Chen, Z.; Chen, P.; Li, S. Effect of Ce addition on microstructure of Al<sub>20</sub>Cu<sub>2</sub>Mn<sub>3</sub> twin phase in an Al-Cu-Mn casting alloy. *Mater. Sci. Eng. A* **2012**, *532*, 606–609. [[CrossRef](#)]



© 2016 by the authors; licensee MDPI, Basel, Switzerland. This article is an open access article distributed under the terms and conditions of the Creative Commons Attribution (CC-BY) license (<http://creativecommons.org/licenses/by/4.0/>).